General Support-Effective Decomposition for Multi-Directional 3-D Printing

Chenming Wu, Chengkai Dai, Guoxin Fang, Yong-Jin Liu, *Senior Member, IEEE*, and Charlie C. L. Wang, *Senior Member, IEEE*

***Abstract*— We present a method for fabricating general models with multi-directional 3-D printing systems by printing different model regions along with different directions. The core of our method is a support-effective volume decomposition algorithm that minimizes the area of the regions with large overhangs. A beam-guided searching algorithm with manufacturing constraints determines the optimal volume decomposition, which is represented by a sequence of clipping planes. While current approaches require manually assembling separate components into a final model, our algorithm allows for directly printing the final model in a single pass. It can also be applied to models with loops and handles. A supplementary algorithm generates special supporting structures for models where supporting structures for large overhangs cannot be eliminated. We verify the effectiveness of our method using two hardware systems: a Cartesian-motion-based system and an angular-motion-based system. A variety of 3-D models have been successfully fabricated on these systems.**

***Note to Practitioners*—In conventional planar-layer-based 3-D printing systems, supporting structures need to be added at the bottom of large overhanging regions to prevent material collapse. Supporting structures used in single-material 3-D printing technologies have three major problems: being difficult to remove, introducing surface damage, and wasting material. This article introduces a method to improve 3-D printing by adding rotation during the manufacturing process. To keep the hardware system relatively inexpensive, the hardware, called a *multi-directional 3-D printing system*, only needs to provide unsynchronized rotations. In this system, models are subdivided into different regions, and then, the regions are printed in different directions. We develop a general volume decomposition algorithm for effectively reducing the area that needs supporting structures. When supporting structures cannot be eliminated, we provide a supplementary algorithm for generating supports compatible with multi-directional 3-D printing. Our method can speed up the process of 3-D printing by saving time in producing and removing supports.**

***Index Terms*— Additive manufacturing (AM), multi-directional 3-D printing, process planning, support, volume decomposition.**

I. Introduction

CONSUMER-GRADE *additive manufacturing* (AM) devices (3-D printers), particularly those based on *fused deposition modeling* (FDM) claim to have the ability to fabricate complex shapes, but the manufacturing process limits their abilities. Fabricating regions with large overhangs requires supporting structures (henceforth, supports) to prevent material collapse. While supports allow fabricating more complex models, they can be difficult to remove, waste material, and damage the model surface [1], [2]. These difficulties greatly reduce the flexibility of 3-D printing in automatic and agile production environments. We develop a 3-D printing system that adds rotational motion into the material accumulation process to enable AM with minimal or no supports.

Various approaches try to overcome the limitation of requiring supports during the fabrication process, such as optimizing the topology of supports (see [3] and [4]), searching for an optimal printing direction [5], and reducing the usage of supports by deformation [6] or model decomposition [7]–[9]. Existing decomposition approaches often fabricate the components of a model separately, requiring a manual "stitching" process to obtain the final result. In other words, they cannot complete the manufacturing process in one pass and, as such, do not need to consider the constraint of collision-free fabrication. We aim to generate the 3-D printing sequence for fabricating a model with one pass along different directions, which we call *multi-directional 3-D printing*. As shown in Fig. 1, our approach can fabricate a model that typically requires a large area of contact supports in a support-free manner.

This article makes the following technical contributions.

1) We formulate the process planning for multi-directional 3-D printing as a volume decomposition problem and summarize the criteria of decomposition.
2) We propose a support-effective volume decomposition algorithm based on the beam-guided search that can be applied to general 3-D models with handles and loops.
3) We develop a region-projection based method to generate supports that are specially designed for multi-directional 3-D printing to address cases where completely support-free fabrication cannot be achieved.

Manuscript received March 16, 2019; revised June 18, 2019; accepted August 8, 2019. Date of publication September 18, 2019; date of current version April 7, 2020. This article was recommended for publication by Associate Editor Z. Xiong and Editor K. Saitou upon evaluation of the reviewers' comments. This work was supported in part by the Seed Fund of TU Delft IDE Faculty, in part by the Natural Science Foundation of China under Grant 61725204, Grant 61521002, and Grant 61628211, in part by the Royal Society-Newton Advanced Fellowship under Grant NA150431, and in part by the MOE-Key Laboratory of Pervasive Computing. *(Corresponding author: Charlie C. L. Wang.)*

C. Wu and Y.-J. Liu are with the Beijing National Research Center for Information Science and Technology, Department of Computer Science and Technology, Tsinghua University, Beijing 100084, China.

C. Dai and G. Fang are with the Department of Design Engineering, Delft University of Technology, 2628 CD Delft, The Netherlands. Part of this work was done when they worked at The Chinese University of Hong Kong, Hong Kong.

C. C. L. Wang is with the Department of Mechanical and Automation Engineering, The Chinese University of Hong Kong, Hong Kong (e-mail: cwang@mae.cuhk.edu.hk).

This article has supplementary downloadable material available at http://ieeexplore.ieee.org, provided by the author.

Color versions of one or more of the figures in this article are available online at http://ieeexplore.ieee.org.

Digital Object Identifier 10.1109/TASE.2019.2938219

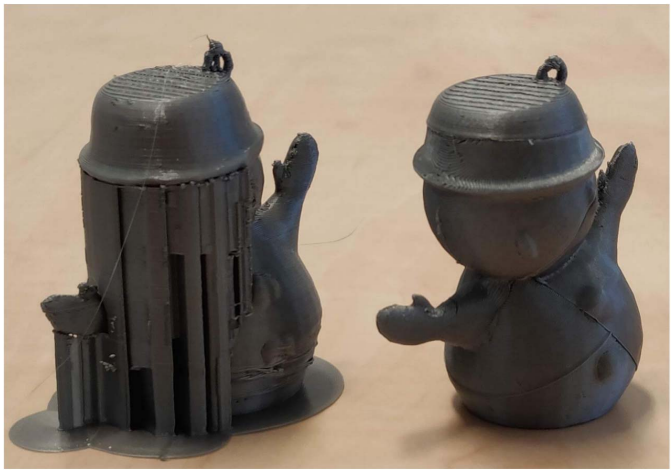

Fig. 1. Snowman models fabricated with an off-the-shelf FDM printer (left) and our multi-directional printing system that adds only one rotational axis to the same printer (right). By allowing material accumulation along different directions in different regions, our system substantially reduces support necessitation.

We developed two types of multi-directional 3-D printing hardware systems: a modified off-the-shelf FDM printer with one additional rotational *degree-of-freedom* (DOF) and an industrial robotic arm that simulates a tilting table, providing two rotational DOFs. Physical fabrications conducted on both systems verify the effectiveness of our method.

II. Related Work

Our work belongs to the interdisciplinary area of geometric computing and multi-axis fabrication, and we review the literature on model decomposition, support-oriented optimization, and multi-axis 3-D printing.

A. Decomposition for Fabrication

Model decomposition is a well-studied geometry processing technique that has recently seen use in 3-D printing applications.

To solve the problem of printing large objects, Luo *et al*. [10] design a framework to decompose large objects that exceed the working envelope of a 3-D printer. They optimize the outcome of segmentation with several objective functions, such as printability, esthetic, and structural soundness. Vanek *et al*. [11] propose an optimization framework that prioritizes reducing printing time and material usage by converting solids into shells and applying a packing step to merge the shells into an optimized configuration for fabrication. Hu *et al*. [9] decompose a model into pyramidal parts for support-free printing. However, pyramidal decomposition is NP-hard so they construct a weak formulation of pyramidal constraints and design an efficient algorithm to solve for the decomposition problem. Herholz *et al*. [7] also try to decompose a model into parts, but instead of following a pyramidal constraint, they allow slight deformation of models to produce pieces in the shape of height fields. RevoMaker [12] can fabricate freeform models on top of an existing electronic component in a cubic shape. Again, the models need to be decomposed into the shape of height-fields. Yao *et al*. [13] develop a level-set method to deal with the problems of partitioning and packing. First, mesh segmentation constructs an initial volume decomposition. Then, their results undergo alternating optimization via an iterative variational optimization method, where partitioning and packing energies are defined in volumetric space. Chen *et al*. [14] also decompose an input model into a small number of parts that can be efficiently packed for 3-D printing. They use an algorithm that explores the decomposition and packing space with a prioritized and bounded beam search guided by local and global objectives.

Staircase artifacts generated by layer-based printing are considered a major type of defect in 3-D printed models. To solve this problem, Wang *et al.* [15] create a method for subdividing the shape into parts that can be built in different directions. After printing all the individual parts, the 3-D printed model is manually assembled, which improves the visual quality by reducing the staircase artifacts. Song *et al*. [16] propose an approach for fabricating large-scale models by combining 3-D printing and laser cutting in a coarse-to-fine fabrication process. Wei *et al*. [17] present a skeleton-based algorithm for partitioning a 3-D shell model into a small number of support-free parts, each of which has a specific printing direction that leads to support-free fabrication. The method also minimizes seams and cracks by integrating the length of the cuts into the optimization formulation. Muntoni *et al*. [8] recently proposed a decomposition algorithm for processing general 3-D objects into a small set of nonoverlapping height-field blocks. The directions of the height fields are constrained to the principal axes to solve the overlapping problem. These blocks can be fabricated by molding or 3-D printing.

None of the discussed decomposition approaches considers the collision-free constraint and sequence of manufacturing. Therefore, they cannot be directly applied to our multi-directional 3-D printing system.

B. Support-Oriented Optimization

Although AM claims to have the ability to fabricate models with complex shapes, the need for supports reduces the flexibility of production. Many prior approaches aim at optimizing either the efficiency of production or the appearance of the model. Several previous works use the volume of supports as an optimization objective for generating effective supports. Vanek *et al*. [4] propose an algorithm for generating hierarchical support structures. MeshMixer [18] also provides a well-designed hierarchical pattern to generate efficient support structures. Dumas *et al*. [3] introduce a bridgelike support structure generation algorithm. Bridges are stronger and more stable than hierarchical structures while still maintaining manufacturing efficiency. However, with the development of fast 3-D printing technology, the contact area of the supports becomes more critical than the volume, which is because a larger contact area requires more effort when manually removing the supports, and the final model retains more surface artifacts.

Another thread of research focuses on changing the 3-D printing orientation to reduce the contact area of supports. Hu *et al*. [6] design an orientation-driven shape deformation framework to adaptively adjust the orientation of regions with large overhangs. Zhang *et al*. [5] propose a double-layered

perceptual neural network (DL-ELM) to rank a list of possible printing directions, with the expectation that the best printing direction prevents critical visual features from being damaged by additional supports. Similar to these works, we introduce rotations into 3-D printing to reduce the number of required supports by minimizing their contact area.

C. Multi-Axis 3-D Printing

Layer-based approaches heavily restrict the flexibility and efficiency of 3-D printing. We review methods for adding more DOFs into the 3-D printing process.

Keating and Oxman [19] present a manufacturing platform using 6-DOF provided by a robotic arm to fabricate models in both additive and subtractive manners. Pan *et al*. [20] propose a 5-axis motion system similar to 5-axis CNC machines to accumulate materials. A 6-DOF parallel kinematic Stewart platform is presented in [21] for multi-directional AM. These systems only fabricate small models with simple shapes. Peng *et al*. [22] propose an *On-the-Fly Print* system to enable fast, interactive fabrication by adding a 2-DOF rotational platform to an off-the-shelf delta 3-D printer. This system can fabricate both solid and wireframe models. Using the *On-the-Fly Print* system, Wu *et al*. [23] propose an algorithm to generate a collision-free printing order for edges in wireframe printing. Huang *et al*. [24] build a robotic arm 3-D printing system based on a 6-DOF KUKA robotic arm and a customized extrusion head. They also propose a divide-and-conquer algorithm to search for a possible fabrication sequence that is both structurally stable and collision-free. Dai *et al*. [25] recently developed a support-free volume printing system equipped with a 6-DOF robotic arm. Shembekar *et al*. [26] present a method for conducting conformal 3-D printing of freeform surfaces by collision-free trajectories, and this method has been validated on a 6-DOF robotic arm. These approaches deposit materials along 3-D tool paths and require relatively expensive devices and control systems to move all DOFs together during the fabrication process. By contrast, our approach decouples the motion for changing orientation from the motion for 3-D printing. As a result, the decomposition generated by our algorithm can be used to supervise the fabrication of general models on a device with meager cost (e.g., the system introduced in Section VI-A).

The decomposition work presented in [27] for $3+2$-axis AM relates closely to our approach. Their work employs a flooding algorithm to segment a given mesh surface into different regions, which can then be fabricated along with different directions without supports. However, this approach is limited in that it only works for treelike models with simple topologies. We propose a more general approach that can process nontreelike models as well as models with handles and loops. Discussion and comparison with [27] can be found in Section VI-C.

III. Methodology

A. Problem Statement

Given a model $\mathcal{M}$ fabricated layer by layer on a base plane π with a printing direction $\mathbf{d}_\pi$, identify whether a face f with normal $\mathbf{n}_f$ is self-supported by

$$e(f,\pi)=\begin{cases}1, & \mathbf{n}_f\cdot\mathbf{d}_\pi+\sin(\alpha_{\max})<0\\ 0, & \text{otherwise}\end{cases} \tag{1}$$

where $\alpha_{\max}$ is the maximal self-supporting angle [6]. Face f is a *risky* face with respect to π when $e(f,\pi)=1$, otherwise it is a *safe* face. Note that $\mathbf{d}_\pi$ is the normal of π. Clearly, the need for supports relates strongly with the printing direction, providing the opportunity for reducing or eliminating supports by changing printing direction during manufacturing.

To supervise the operating multi-directional 3-D printer, we need to generate a decomposition of $\mathcal{M}$, where

1) $\mathcal{M}$ has N components such that
$$\mathcal{M}=\mathcal{M}_1\cup\mathcal{M}_2\cup\cdots\cup\mathcal{M}_N=\cup_{i=1}^{N}\mathcal{M}_i \tag{2}$$
with $\cup$ denoting the *union* operator;
2) $\{\mathcal{M}_{i=1,\ldots,N}\}$ is an ordered sequence that can be collision-freely fabricated with
$$\pi_{i+1}=\mathcal{M}_{i+1}\cap\left(\cup_{j=1}^{i}\mathcal{M}_j\right) \tag{3}$$
being the base plane of $\mathcal{M}_{i+1}$—here $\cap$ denotes the *intersection* operator;
3) π_1 is the working platform of a 3-D printer;
4) all faces on a subregion $\mathcal{M}_i$ are *safe* according to $\mathbf{d}_{\pi_i}$ determined by π_i.

We solve the weak-form problem by reducing the area of risky faces on each component $\mathcal{M}_i$, that is, minimize

$$J_G=\sum_i\sum_{f\in\mathcal{M}_i}e(f,\pi_i)A(f) \tag{4}$$

where $A(f)$ is the area of face f. While minimizing the objective function (4), we need to ensure the fabricating each component is collision-free. For regions where faces are not entirely safe, we generate supports specially designed for multi-directional 3-D printing.

B. Our Approach

Multi-directional 3-D printing a given model $\mathcal{M}$ requires determining an ordered sequence of clipping planes γ_k $(k=1,\ldots,N-1)$ that decomposes $\mathcal{M}$ into N components [see Fig. 2(a)]. We define the half-space of a clipping plane γ_k containing the 3-D printing platform $\mathcal{P}$ as "below," denoted by Γ_k^-) and the half-space "above" γ_k is Γ_k^+. The clipping operation gives the remained model by

$$\bar{\mathcal{M}}_k=\bar{\mathcal{M}}_{k-1}\setminus\Gamma_k^+ \tag{5}$$

with $\bar{\mathcal{M}}_0=\mathcal{M}$ and "\" denotes the subtraction operator on solids. When every clipped subregion in Γ_k^+ satisfies the criteria of manufacturability (see Section III-C), the inverse order of clipping gives the sequence of region printing for multi-directional 3-D printing. Specifically, we have

$$\mathcal{M}_i=\bar{\mathcal{M}}_{(N-i)}\cap\Gamma_{(N-i+1)}^+,\quad \pi_i=\gamma_{(N-i+1)} \tag{6}$$

with $i=1,\ldots,N$. The printing direction of a subregion $\mathcal{M}_i$ is given by the normal vector of γ_k pointing from Γ_k^- into Γ_k^+ with $k=N-i+1$. Fig. 2(b) shows an illustration of

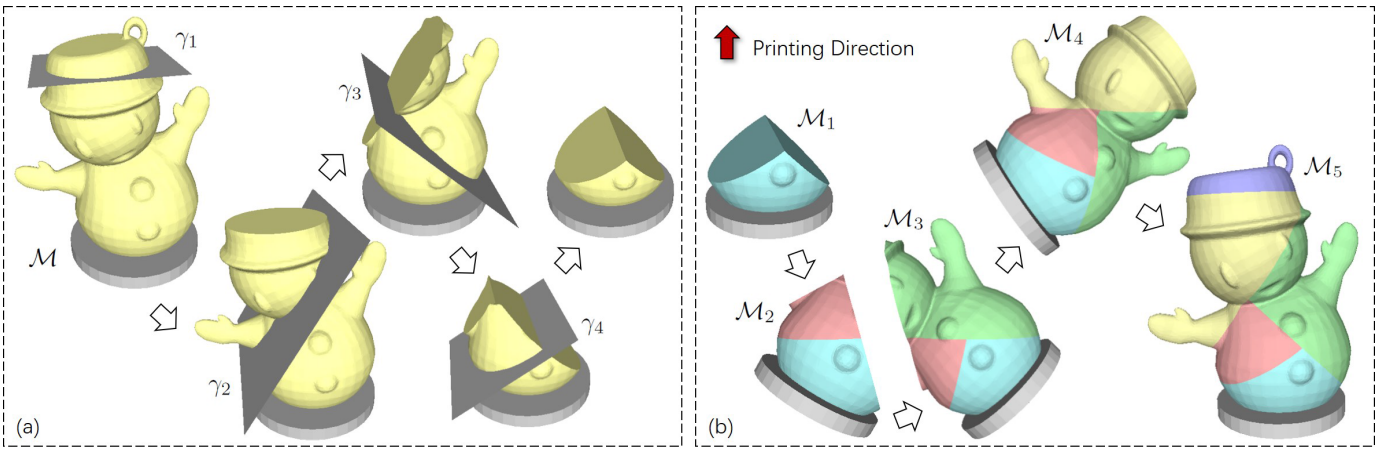

Fig. 2. Illustration for our algorithm. (a) Progressively determined results of planar clipping for generating the optimized decomposition. (b) Inverse order of clipping planes that result in a sequence of regions for fabrication. The printing direction of each region is the normal of its base plane. Note that the orientation of a printing head is fixed during the procedure of physical fabrication, and the parts under fabrication are reoriented to realize the multi-directional 3-D printing.

using the inverse order of clipping to obtain the sequence for multi-directional 3-D printing. Half-spaces defined by sequentially applying all N clipping operations subdivide the $\Re^3$ space into $N+1$ convex subspace. The first k clipping operations generate the $\mathcal{M}_i$ component (6) in a subspace as in

$$\Omega_k = \Gamma_1^- \cap \Gamma_2^- \cap \cdots \cap \Gamma_{k-1}^- \cap \Gamma_k^+ = \left(\cap_{j=1}^{k-1} \Gamma_j^-\right) \cap \Gamma_k^+ \quad (7)$$

with $\Omega_1 = \Gamma_1^+$. When needed, the supporting structure for the component $\mathcal{M}_i$ will be generated in Ω_k $(k = N - i + 1)$ and progressively projected into the rest subspace Ω_j $(j > k)$ until it can be merged with other supports or meets the printing platform $\mathcal{P}$ (see Section V for details).

Candidates of clipping planes can be generated by

1) uniformly sampling the Gaussian sphere to obtain 250 normals;
2) applying a uniform shifting along each sampled normal vector with an offset of 1 mm.

For all examples shown in this article, this sampling strategy generated around 15k–20k candidate clipping planes. We develop a beam-guided search scheme to select an optimized order of clipping, which can significantly improve the local-optimum results obtained from a greedy scheme. Details will be presented in Section IV.

The planar clipping methodology employed in this article can process general models with a high-genus number, addressing the drawbacks in [17], [27], and [28], which could only process models with skeletal-tree structures. In addition, the algorithm can be easily tailor-made to support a hardware system with only one rotational axis [e.g., the system shown in Sec. VI(A)]. This is realized by generating samples $\mathbf{n}_k$ on a circle of the Gaussian sphere satisfying $\mathbf{n}_k \cdot \mathbf{r} = 0$ with $\mathbf{r}$ being the axis of rotation. Moreover, we provide a support generation solution to enable the fabrication of all models on a multi-directional 3-D printing system.

C. Criteria for Decomposition

We now define the criteria for finding an optimal subregion $\mathcal{M}_i$ according to a clipping plane γ_k $(k = N - i + 1)$ for multi-directional 3-D printing. Here π_i denotes the corresponding base plane of γ_k.

Criterion I: $\forall f \in \mathcal{M}_i$, $e(f, \pi_i) = 0$—i.e. all faces on $\mathcal{M}_i$ are self-supported.

Minimization of the objective function (4) imposes this criterion, ensuring the manufacturability of the region above γ_k.

Criterion II: The model $\bar{\mathcal{M}}_k$ obtained from the clipping by γ_k must be connected to the printing platform $\mathcal{P}$.

This criterion prevents unmanufacturable configurations for the region below γ_k by avoiding the generation of "floating" regions, which require supports when printed.

The next criterion avoids collisions between the printer head and the platform.

Criterion III: The printing platform $\mathcal{P}$ and the clipping plane γ_k satisfy $\Gamma_k^+ \cap \mathcal{P} = \emptyset$ (i.e., $\mathcal{P}$ is below γ_k).

Note that we do not explicitly prevent collision between the printer head and already fabricated regions as the clipping routine that generates subregions from $\mathcal{M}$ already guarantees this. All regions $\mathcal{M}_{j\,(j<i)}$ are below the base plane π_i (i.e., the clipping plane $\gamma_{(N-i+1)}$) because the sequence of 3-D printing is the inverse order of clipping.

In practice, we cannot always find a decomposition satisfying Criterion I for all components. For such a scenario, a weak form for support-free is adopted to aim at generating a smaller area of overhang during fabrication.

When changing from one printing direction to another printing direction, the following drawbacks are introduced.

1) The visual artifact of a curve is formed at the interface of two neighboring regions.
2) It takes extra time for the machine to move from one orientation to the other—the printing process is slower.

Therefore, we generally prefer a solution with fewer components, which can be achieved by considering the following criterion of clipping.

Criterion IV: We prefer a large solid volume for the region above a clipping plane.

In summary, the volume decomposition of $\mathcal{M}$ is considered *optimized* when it satisfies all the above-mentioned criteria. Two schemes developed in Section IV compute the optimal decomposition.

IV. Schemes of Optimization

We introduce greedy and beam-guided search schemes for determining the sequence of clipping planes and thereby obtaining the corresponding volume decomposition. The beam-guided search scheme avoids converging at local optima.

A. Greedy Scheme

Consider a clipping plane γ that decomposes the current model $\bar{\mathcal{M}}_c$ into the upper and lower parts, $\bar{\mathcal{M}}_c^+$ and $\bar{\mathcal{M}}_c^-$. A greedy scheme searches for a γ that most significantly reduces the current value of the global objective function [i.e., J_G in (4)]. To implement this strategy, we define a local objective function as a weak form of Criterion I, which evaluates the descent of risky areas, by

$$\begin{aligned} J_L &= \sum_{f\in\bar{\mathcal{M}}_c} e(f,\pi(\mathcal{P}))A(f) \\ &\quad - \left(\sum_{f\in\bar{\mathcal{M}}_c^-} e(f,\pi(\mathcal{P}))A(f) + \sum_{f\in\bar{\mathcal{M}}_c^+} e(f,\pi(\gamma))A(f)\right) \\ &= \sum_{f\in\bar{\mathcal{M}}_c^+} (e(f,\pi(\mathcal{P})) - e(f,\pi(\gamma)))A(f) \end{aligned} \tag{8}$$

where $\mathcal{P}$ is the platform of a 3-D printer.

Among all the candidate clipping planes, the greedy scheme always selects the plane with maximum J_L

$$\gamma = \arg\max J_L(\gamma). \tag{9}$$

However, such a selection does not guarantee the region $\bar{\mathcal{M}}_c^+$ above the selected clipping plane is completely support-free. To address this, we propose a constrained greedy scheme. The clipping plane is selected by

$$\gamma = \arg\max J_L(\gamma) \quad \text{s.t. } R(\mathcal{M}_c^+,\gamma) = 0 \tag{10}$$

with

$$R(\mathcal{M}_c^+,\gamma) = \sum_{f\in\bar{\mathcal{M}}_c^+} e(f,\pi(\gamma))A(f) \tag{11}$$

giving the total area of risky faces on $\mathcal{M}_c^+$.

In practice, we first select candidates among the clipping planes that let $\mathcal{M}_c^+$ be completely self-supported. If there is no such a clipping plane, we solve a degenerated problem (9). After adding this preference for support-free regions, the objective function J_G can be further minimized on most models (as shown in Fig. 3). However, counterexamples can also be found where the additional constraint increases J_G—e.g., the snowman. This is mainly because a greedy scheme can easily fall into a local optimum. A better search scheme needs to be developed by considering all the criteria discussed in Section III-C.

B. Beam-Guided Search Scheme

As aforementioned, in many cases, it is not guaranteed to find a support-free decomposition for every subregion—i.e., Criterion I is not satisfied for some regions. To provide a general solution, we reformulate this criterion into a weak form as a local objective function. Specifically, we search for a clipping plane γ_k that leads to

$$\min R(\mathcal{M}_{N-k+1},\gamma_k) \tag{12}$$

with $R(\cdot,\cdot)$ evaluating the total area of risky faces as defined in (11). Criteria II and III are imposed by excluding those unsatisfactory clipping planes from the set of candidates. Similarly, to avoid generating too many small fragments when decomposing an input model $\mathcal{M}$, clipping operations that lead to a subregion with volume less than $V(\mathcal{M})/w$ are prevented. Here, w is a user-specified parameter to control the maximal number of components (i.e., w from 10 to 12 is used in our tests).

Beam search [29] is an efficient search technique that has been widely used to improve the results of the best-first greedy search. A breadth-first strategy is employed to build a search tree that explores the search space by expanding the set of most promising nodes instead of only the best node at each level. It has been successfully used in a variety of areas, especially in geometric configuration search tasks for 3-D printing (see [10], [14]). Our approach introduces a progressive relaxation routine to conduct the breadth-first search.

The most challenging part in solving our volume decomposition is integrating the restrictive Criterion I (and its weak form) as an objective function presented in (12). This important step ensures that the beam search is broad enough to include both the local optimum and configurations that may lead to a global optimum. In contrast with the traditional usage of a beam search algorithm that keeps the b most promising results, our beam-guided search algorithm starts from an empty beam with the most restrictive requirement of $R(\mathcal{M}_{N-k+1},\gamma_k) < \delta$, where δ is a tiny number (e.g., $\delta = 0.1$ is used in all our tests). Candidate clipping planes that satisfy this requirement and remove larger areas of risky faces have higher priority when filling the b beams. If there are still empty beams, we relax δ by letting $\delta = 5\delta$ until all b beams are filled. Details of our beam-guided search algorithm are presented in the following.

The algorithm starts from b empty beams $\mathcal{B}^j$ ($j = 1,\ldots,b$), where each beam $\mathcal{B}^j = (\mathcal{M}(\mathcal{B}^j), \mathcal{L}(\mathcal{B}^j))$ contains a remaining model $\mathcal{M}(\mathcal{B}^j)$ and an ordered list of clipping planes, $\mathcal{L}(\mathcal{B}^j)$, that forms $\mathcal{M}(\mathcal{B}^j)$. In our implementation, only the last element of a list needs to be stored in $\mathcal{B}^j$, as the rest of the prior elements in the list can be traced through a backward link. By using the progressive relaxation routine, each beam can be extended by adding a new clipping plane into its list and obtaining an updated remaining model. In the next round, apply progressive relaxation to all valid clipping results for all b remaining models, prioritizing the removal of more risky faces. Repeat the extension process of beam $\mathcal{B}^j$ until any of the following terminal conditions is satisfied on the remaining model $\mathcal{M}(\mathcal{B}^j)$.

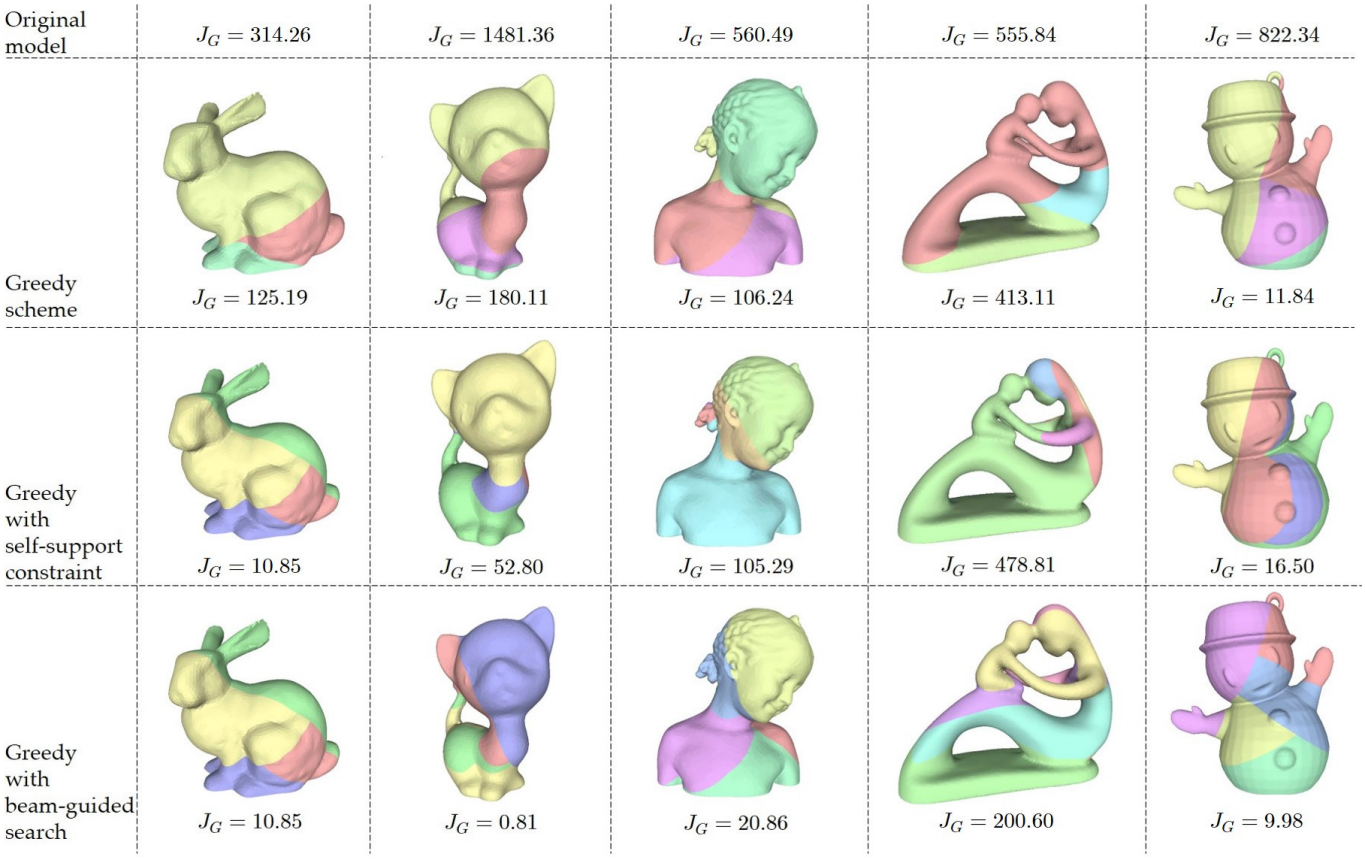

Fig. 3. Comparison of decomposition results obtained from three schemes introduced in this article. Beam-guided search always determines the "best" decomposition (i.e., the one with minimized J_G (4).

1) *Small Volume*: The volume of the remaining model $\mathcal{M}(\mathcal{B}^j)$ has small volume—i.e., $V(\mathcal{M}(\mathcal{B}^j)) < (1/w)V(\mathcal{M})$.
2) *Self-Supported*: The remaining model $\mathcal{M}(\mathcal{B}^j)$ is completely self-supported as $R(\mathcal{M}(\mathcal{B}^j), \pi(\mathcal{P})) = 0$.

The search also terminates when no beam can be further extended.

Each beam corresponds to a list of clipping planes that gives a decomposition model $\mathcal{M}$. The decomposition that leads to the minimal value of J_G (4) is considered the optimized solution for our multi-directional 3-D printing. Pseudocode of our beam-guided search algorithm is given in Algorithm 1. We use the method of discarding results close to already selected ones, which is proposed in [10], to avoid filling the beam by similar results. Example results and a comparison against two other greedy (constrained and unconstrained) schemes can be found in Fig. 3. The beam-guided search gives the best decomposition on all models.

V. Support Generation

After relaxing the hard constraint of creating a support-free model decomposition into minimizing the area of risky faces, J_G, the scheme for generating supports is considerately important for models that still have risky faces after decomposition. To tackle this problem, we propose a new structure called *projected support* that ensures the fabrication of remaining overhanging regions through collision-free multi-directional 3-D printing.

For a decomposition that results in a sequence of subregions $\mathcal{S} = \{\mathcal{M}_i\}$ with base plane π_i corresponding to each subregion $\mathcal{M}_i$, the printing direction $\mathbf{d}_i$ is the normal vector of π_i. Thus, the overhanging region on $\mathcal{M}_i$ with respect to the printing direction $\mathbf{d}_i$ can be detected and supporting structures added along the direction $(-\mathbf{d}_i)$. Here, we select the treelike support [4] that merges the supporting structures for different overhanging regions when they are near each other. In fact, our progressive projection algorithm is general and can be applied to different patterns of supports, such as the bridgelike support [3] or other denser supports [30].

Unlike the existing algorithms that generate supports by projecting along a fixed printing direction, in our case, the projection should be conducted along with different directions in different regions. Without loss of generality, the ith component $\mathcal{M}_i$ falls in a subspace $\mathbf{\Omega}_k$ formed by the first k clipping planes, as shown in (7) with $k = N - i + 1$. The support for the overhang on $\mathcal{M}_i$ is generated along the inverse printing direction $(-\mathbf{d}_i)$ and projected onto the base plane (i.e., the kth clipping plane, γ_k). Next, the structure is projected into a new subspace $\mathbf{\Omega}_{k+1}$ and along a new direction $(-\mathbf{d}_{i-1})$. The projection repeats until this structure can be merged with other structures or meets the printer's platform $\mathcal{P}$. Fig. 4(b) shows supports generated by our progressive projection algorithm displayed in different colors when they are in different

Algorithm 1: Beam-Guided Search

Input: Input mesh $\mathcal{M}$.
Output: An optimized set of decomposition as $\{\mathcal{M}_i\}$.

Build a set of uniformly sampled candidate planes Π (Section III-B) that $\forall \gamma \in \Pi,\ \gamma \cap \mathcal{P} = \emptyset$ (Criterion III);
Initialize b empty beams as $\forall j,\ \mathcal{B}^j = (null, null)$;
$\mathcal{B}^1 = (\mathcal{M}, null)$;
repeat
  /* Preparing clipping candidates */
  Initialize a maximum heap of clipping as $\mathcal{G} = \emptyset$;
  forall the $\mathcal{B}^j$ **do**
    if $\mathcal{M}(\mathcal{B}^j) \neq null$ **then**
      forall the $\gamma \in \Pi$ **do**
        The clipping plane γ decomposes $\mathcal{M}(\mathcal{B}^j)$ into $\mathcal{M}^+$ and $\mathcal{M}^-$;
        if $(V(\mathcal{M}^+) \geq \frac{1}{w} V(\mathcal{M}))$ *AND* ($\mathcal{M}^-$ *is connected to* $\mathcal{P}$) **then**
          Evaluate J_G according to $\mathcal{L}(\mathcal{B}^j)$;
          Insert the tuple $(\mathcal{M}^-, \mathcal{M}^+, \mathcal{L}(\mathcal{B}^j), \gamma)$ into $\mathcal{G}$ with J_G as the key;
        end
      end
    end
  end
  /* Progressive relaxation */
  $\delta = 0.1$ and $k = 0$;
  while $k < b$ **do**
    Initialize a maximum heap $\bar{\mathcal{G}}$ as buffer;
    while $\mathcal{G} \neq \emptyset$ **do**
      Pop $(\mathcal{M}^-, \mathcal{M}^+, \mathcal{L}, \gamma)$ from the top of $\mathcal{G}$;
      if $R(\mathcal{M}^+, \gamma) < \delta$ **then**
        Add γ at the tail of $\mathcal{L}$;
        Let $\mathcal{B}^{k+1} = (\mathcal{M}^-, \mathcal{L})$ and $k = k + 1$;
      else
        Evaluate J_G according to $\mathcal{L}$;
        Insert the tuple $(\mathcal{M}^-, \mathcal{M}^+, \mathcal{L}, \gamma)$ into $\bar{\mathcal{G}}$ with J_G as the key;
      end
    end
    Let $\mathcal{G} = \bar{\mathcal{G}}$ and $\delta = 5\delta$;
  end
  /* Checking terminal condition */
  forall the $\mathcal{B}^j$ **do**
    if $(V(\mathcal{M}(\mathcal{B}^j)) < \frac{1}{w} V(\mathcal{M}))$ *OR* $(R(\mathcal{M}(\mathcal{B}^j), \pi(\mathcal{P})) = 0)$ **then**
      Evaluate J_G according to $\mathcal{L}(\mathcal{B}^j)$;
      $\mathcal{B}^j = (null, \mathcal{L}(\mathcal{B}^j))$;
    end
  end
until $\forall j,\ \mathcal{M}(\mathcal{B}^j) = null$;
return the decomposition that gives the minimal J_G;

subspaces $\{\Omega_k\}$. The pseudocode of our progressive projection algorithm is given in Algorithm 2.

After applying the volume decomposition algorithm, we use the uniformly sampling strategy to detect all overhang types—including point-overhang, edge-overhang, and face-overhang. Sampling interval R is a parameter selected by the diameter of the deposition nozzle and struts. We use $R = 3$ mm for printing with a 0.8-mm-diameter nozzle and $R = 2$ mm for printing with a 0.4-mm-diameter nozzle. For each submesh $\mathcal{M}_s$ and its associated subspace Ω_s, an ideal configuration of support structures $\mathcal{C}_s$ should satisfy $\mathcal{C}_s \subset \Omega_s$ with a minimal number of points that contact the input model. We use the method proposed in [4] to ensure that the newly generated nodes of the tree are inside Ω_s during the merging procedure. This guarantees that the corresponding connected structures are inside the convex space Ω_s. We set the maximal self-supporting angle for sparse treelike supports to 30° and adopt a heuristic greedy-based method [4] to progressively merge pairs of supporting structures when they are close to each other.

Moreover, considering the stability issue raised by gravitational torque when printing along with different directions, we propose the following function for selecting the diameter R_p of a projected supporting strut $\mathcal{C}_p \subset \Omega_k$:

$$R_p = \left(1 + \lambda \left\| \sum_i V_i(\mathbf{c}_i \times \mathbf{g}) \right\|\right) R/4 \tag{13}$$

where $\| \sum_i V_i(\mathbf{c}_i \times \mathbf{g}) \|$ is the torque on top of $\mathcal{C}_p$, and $\mathbf{c}_i$ and V_i are the centroid and the volume of the supporting strut connected to $\mathcal{C}_p$. λ is a user-defined parameter to determine

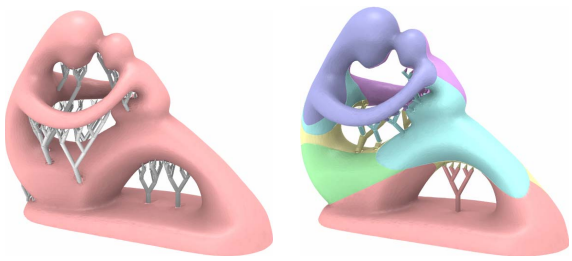

(a) (b)

Fig. 4. (a) Sparse treelike supporting structures for 3-D printing along with a fixed direction. (b) Progressively projected supports generated by our algorithm for multi-directional 3-D printing. Note that fewer supports are needed for the multi-directional printing. To avoid the issues of stability raised by gravitational torques, we incorporate dynamic struts defined in (13) to generate projected support structures in our system.

Algorithm 2: Progressive Projection

Input: Components of $\mathcal{M}$ in a sequence $\mathcal{S}$.
Output: Support structures $\mathcal{T}$

Initialize an empty set $\mathcal{T} = \emptyset$ for support-structures;
for $i = N, \ldots, 1$ **do**
  if $R(\mathcal{M}_i, \pi_i) > 0$ **then**
    Generate support $\mathcal{C}_i$ for $\mathcal{M}_i$ inside Ω_{N-i+1};
    Merge $\mathcal{C}_i$ into $\mathcal{T}$;
  end
  Extend $\mathcal{T}$ along the direction of $(-\mathbf{d}_i)$ until meeting the base plane π_i or the component $\mathcal{M}_i$;
end
return $\mathcal{T}$;

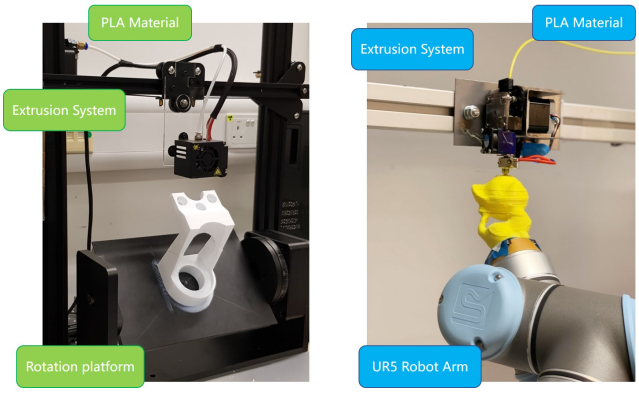

Fig. 5. Two different hardware setups for multi-directional printing have been built to verify the effectiveness of our volume decomposition approach. A Cartesian-space-based 4-DOF printer modified from an off-the-shelf FDM printer with an additional DOF to provide the capability of rotation (left). A joint-space-based 5-DOF system consisting of an industrial 6-DOF robotic arm and a fixed FDM extruder (right).

the diameter of projected supports, and we empirically set it as 10^{-6}.

VI. Experimental Results

We have implemented the proposed search algorithms in C++ and Python programs and tested them on a PC with two Intel E5-2698 v3 CPUs and 128-GB RAM. To prove the effectiveness of our algorithm, we use a conservative choice of the maximal self-supporting angle as $\alpha_{\max} = 45°$. In practice, this parameter highly depends on a 3-D printer's capability, and up to 70° can be achieved by advanced 3-D printers, such as the one used in [17]. The slicing software for conventional FDM, Ultimaker Cura [31], is used to create planar slices and tool-paths according to the printing directions determined in our algorithm. The generated g-code for fabrication is sent to the motion-control module of the hardware. Two different hardware platforms have been used to verify the effectiveness of decomposition, with different configurations for navigating the motions of material extrusions. One is a Cartesian-space-based system with 4-DOF in motion, and the other hardware platform is a joint-space-based system [28] that is built on an industrial robotic arm equipped with a fixed FDM extruder.

A. Cartesian-Space-Based Hardware

The hardware setup of the 4-DOF multi-directional printer is developed on top of an off-the-shelf FDM printer (i.e., Creality CR-10S and Ultimaker 2+) by adding a rotational platform. Inspired by the 4-axis CNC machine, a turbine-shaft structure driven by a step-motor is built vertically and fixed into the base of the 3-D printer platform, which will be moved together. Note that the additional cost of this hardware system is only about 240 USD, which is cost-effective when comparing to devices with synchronized multi-axis motion. Moreover, we design an easy-to-calibrate platform, shown in Fig. 5 (left), which allows ±60° collision-free rotation.

During the manufacturing process, the motion of the printer header is fully controlled by the 3-D printer itself. The newly added motor for rotation is only used to realize the orientation change between submodels from one to the next. An Arduino chipboard controls the rotation applied to the platform of 3-D printing. Note that as a step motor is used, only a limited number of orientations can be realized. This manufacturing constraint is considered while generating sample points on the Gaussian sphere for clipping planes.

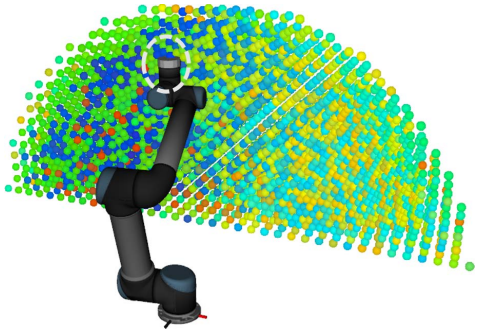

Fig. 6. Reachability map of our robotic arm, where different colors represent different levels of reachability (i.e., from worst to best in colors red, yellow, green, skyblue, and blue). The fixed FDM extruder is placed at the center of a region with high reachability (i.e., the region circled in dash lines).

B. Joint-Space-Based Hardware

The principle of the 4-DOF system can also be extended to 5-DOF by using a tilting table with two rotational DOFs (Fig. 5 (right)). In our experimental tests, a 6-DOF robotic arm is used to demonstrate the functionality of our method with 5-DOF motion, although a robotic arm provides much lower positioning accuracy. The hardware setup is composed of a UR5 robotic arm, an FDM extruder fixed on a frame, and some other control components. As the extruder is fixed to obtain better adhesion in our system, the change in printing directions and positions is realized by the inverse poses of a printing platform attached to the UR5 robotic arm. Considering the accuracy of positioning that can be achieved on UR5 [32] and the speed of fabrication, we employ a 0.8-mm-diameter nozzle in our system for material deposition.

Because of the hardware constraints of the UR5 robotic arm (e.g., limited ranges of joints), not every point with a given orientation can be realized. The reachability of points inside the working envelope is very sensitive to the relative position of the nozzle in the coordinate system of the UR5's base frame, which needs to be optimized to enhance the reachability. First, the workspace of a robotic arm is uniformly sampled into points. For each point in the Cartesian space, we randomly sample an additional 100 points on the unit sphere around the point with orientations toward the center of the sphere. The reachability map can be generated by Reuleaux [33]. As shown in Fig. 6, we placed the extruder of our setup at the center of a region with the highest reachability.

C. Results and Discussion

Fig. 7 (top row) shows the process of 3-D printing of the 4-DOF system. Fig. 7 (middle and bottom rows) presents

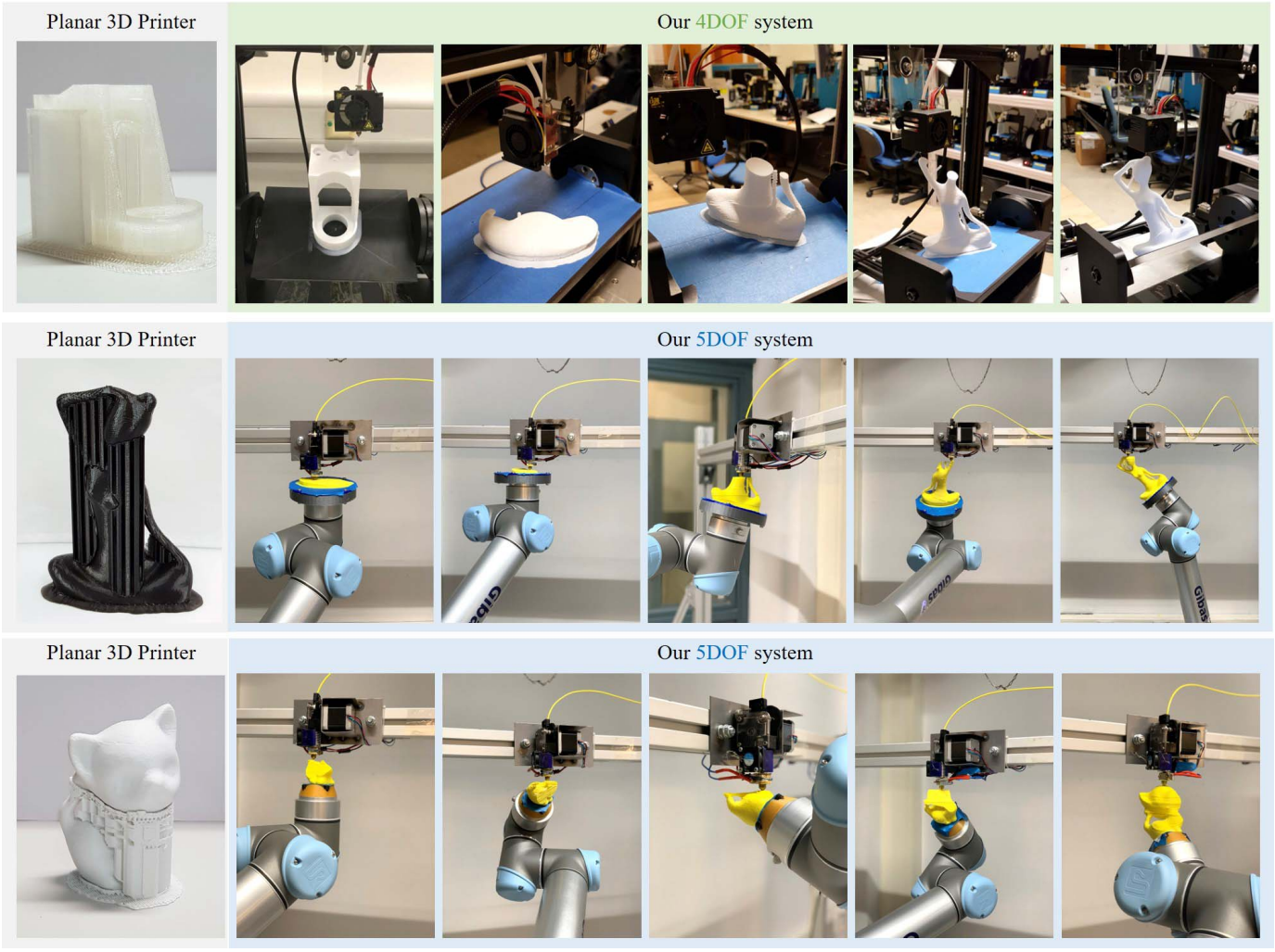

Fig. 7. Progressive results of fabricating models with our 4-DOF multi-directional 3-D printing system (top row) and a 5-DOF system realized on a robotic arm (middle and bottom rows).

the progressive results of models fabricated on the 5-DOF multi-directional 3-D printing system. Our method can successfully decompose a given model into support-free components to be fabricated one by one.

We applied our volume decomposition algorithm to a variety of models. In addition to the models shown in Figs. 1 and 3, we tested our system on models with higher genus-number (see Figs. 7 and 8). Our algorithm can greatly reduce or even eliminate the need for supports on these models. Models that still require supports add these supports to only very small regions of the model, and we compare these results to a conventional planar 3-D printer in Fig. 7.

The major advantage of our approach compared with that in [27] is the ability to handle models with handle and loop topology (see the models in Fig. 8). For example, when applying the algorithm of Xu *et al.* [27] to the Kitten model in Fig. 8, their flooding algorithm is stuck at the fourth region, as shown in Fig. 9. When applying their method to the Bunny model with genus-zero topology, the result is similar to ours (see Fig. 10), though our result has a slightly smaller J_G. Another problem with their method is that the collision-free constraint has not been explicitly incorporated into the computation—i.e., the collision between the printer head and the already fabricated ear may happen when printing the other ear of the Bunny.

Letting $J_G = 0$ is *sufficient* but *unnecessary* for a model $\mathcal{M}$ to be support-freely fabricated by the multi-directional 3-D printing system. In other words, when our algorithm returns a decomposition with $J_G \neq 0$ for a model, it is still possible to have a solution for support-free decomposition that was not found. This is partially because of the local optimum determined by the beam-guided search. Our sampling strategy discretizes continuous 3-D space, which can also raise this problem.

When generating submodels for 4-DOF printing, the resulting decomposition depends on the selection of the rotational axis. As shown in Fig. 11, when specifying different axes, e.g., $\mathbf{r}_a = (1, 0, 0)$ and $\mathbf{r}_b = (0.829, -0.559, 0)$ as rotational axis, the decomposition results in different levels of self-support. Specifically, we obtain $J_G = 126.58$ and $J_G = 87.33$ when using $\mathbf{r}_a$ and $\mathbf{r}_b$ as the rotation axis, respectively. This brings in a new parameter, the rotational axis, to further

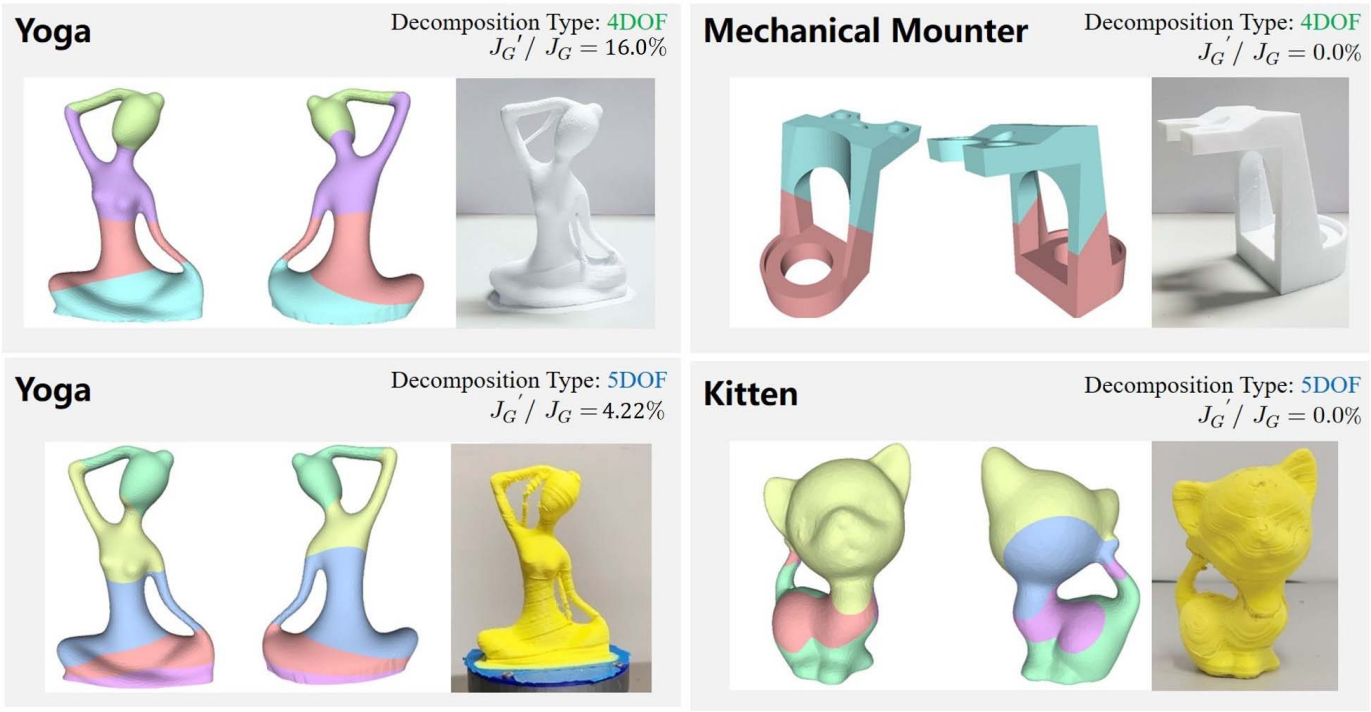

Fig. 8. Decomposition results fabricated by our system with 4-DOF and 5-DOF in motion, where the resultant value of J_G is also reported.

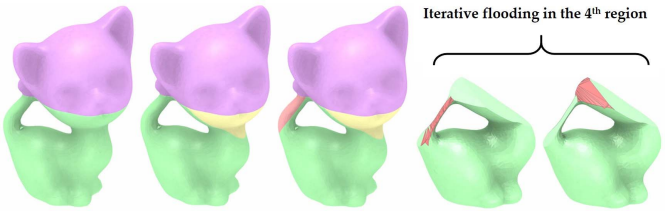

Fig. 9. Progressive result of applying the flooding-based algorithm [27] to the Kitten model, which is stuck at the fourth region due to handle topology.

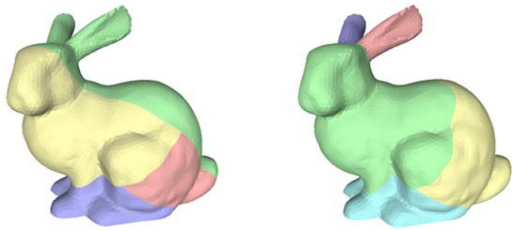

Fig. 10. Comparison of our result (left with $J_G = 10.85$) and the result in [27] (right with $J_G = 31.55$).

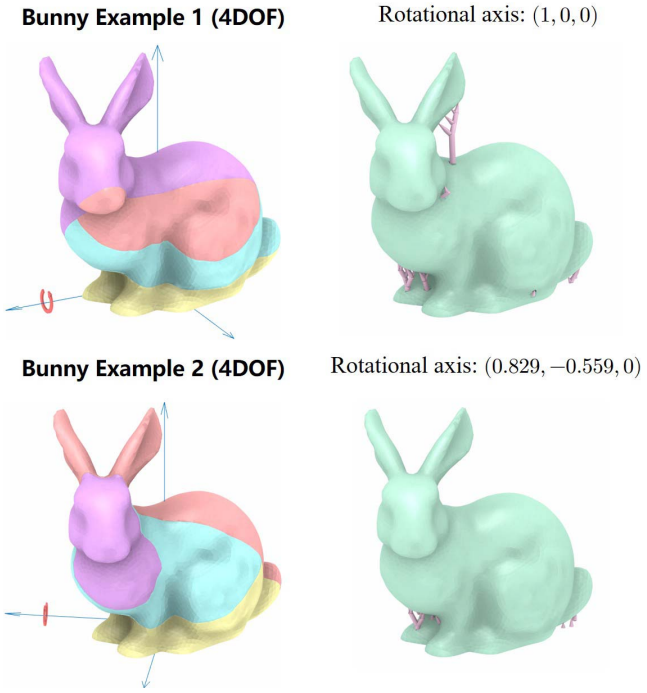

Fig. 11. When selecting different axes for 4-DOF fabrication, the decomposition gives different results—(left) $J_G = 126.58$ for using $(1, 0, 0)$ as the rotational axis and (right) $J_G = 87.33$ for rotating around $(0.829, -0.559, 0)$. The rotational axes are shown in red. As can be found in the top row, supporting structures need to be added below the ear of the bunny by the rotational axis $(1, 0, 0)$. This is eliminated by using $(0.829, -0.559, 0)$ as the rotational axis (see the bottom row).

optimize the decomposition. A simple solution is to discretely sample a few possible rotational axes and then select the one that leads to the minimal J_G after decomposition.

Our approach employs a sampling strategy for generating candidates of clipping planes, which are then used for computing the decomposition and sequence of multi-directional 3-D printing. In one way, this helps us impose manufacturing constraints easily—e.g., limiting the rotational axis, computing orientations that can be physically realized by step-motors, and excluding the singular and the collided poses for a robotic arm. On the other hand, this also limits the space of computation. The variables in our computations are not continuous, which means we may miss the "real" optimal

TABLE I
COMPUTATIONAL STATISTIC

Model	Fig.	Trgl. #	Type	Computing Time	Part #	J_G		Support Volume		Printing Time	
						Before	After	*Fixed Dir.*	*Multi-Dir.*	*Fixed Dir.*	*Multi-Dir.*
Bunny	3	12,420	5DOF	94 sec.	5	314.26	10.85	130.59	0.00	42 min.	55 min.
Kitten	3	10,000	5DOF	98 sec.	5	1481.36	0.81	893.58	0.00	220 min.	187 min.
Bimba	3	12,156	5DOF	105 sec.	5	560.49	20.86	382.46	14.42	108 min.	134 min.
Fertility	3	16,172	5DOF	314 sec.	6	555.84	200.60	310.25	156.53	59 min.	70 min.
Snowman	3	10,000	5DOF	104 sec.	5	822.34	9.98	370.92	7.33	188 min.	240 min.
	1		4DOF	64 sec. (Total: 192 min.)	5		11.84		12.62		242 min.
Yoga	8	11,254	5DOF	298 sec.	5	613.89	25.92	392.17	39.92	189 min.	234 min.
	8		4DOF	88 sec. (Total: 266 min.)	4		98.51		74.56		207 min.
Mechanical-Mounter	8	15,348	5DOF	52 sec.	2	698.09	0.00	843.45	0.00	56 min.	39 min.
	8		4DOF	34 sec. (Total: 102 min.)	2		0.00		0.00		39 min.

clipping planes. To address this, future work should consider further adjusting clipping planes via continuous optimization by using the planes determined in our approach as an initial guess.

Table I gives the computational statistics of models tested in this article. For the 4-DOF decomposition, we report both the average time for the beam search according to a given rotational axis and the total time for searching all possible rotational axes (reported in the bracket), where 180 possible rotational axes are considered. The computational efficiency of our approach is acceptable when compared with the 3-D printing time (i.e., around a few hours in general). We measure printing time using Ultimaker Cura (Version 3.6.0) [31] with the settings of 0.4-mm layer height and 20% grid infill. The volumes of support needed for 3-D printing along a fix direction (denoted by *Fixed Dir.*) and our method (denoted by *Multi-Dir.*) are reported in Table I. We also report the comparison of printing time. The reason why longer time is needed for multi-directional 3-D printing on some models is the hollowed volume is less on the decomposed components.

Another weakness of this decomposition-based multi-directional 3-D printing approach is the relatively weak stiffness of the model. As already studied in [28], smaller Young's modulus is observed on the specimens generated by this approach during the tensile tests. The weak adhesion of materials mainly causes this at the interface between two regions. One of our future research questions is how to design special structures at the interface between different regions to enhance the mechanical strength of adhesion.

VII. CONCLUSION

We present a volume decomposition framework for the support-effective fabrication of general models via multi-directional 3-D printing. A beam-guided search computes the decomposition while avoiding local optima. While prior work can only fabricate models with skeletal tree structures, our method can apply to models with multiple loops and handles. We also provide a support generation scheme that allows our framework to fabricate all types of models. The framework can incorporate manufacturing constraints such as the number of rotational axes and the realizable configurations during the orientation sampling process. As a result, our algorithm supports both the 4-DOF and 5-DOF systems. We verify the effectiveness of our approach by creating a variety of models on multiple hardware setups.

ACKNOWLEDGMENT

The authors would like to thank N. Haduong from the University of Washington for polishing the writing.

REFERENCES

[1] W. Gao *et al.*, "The status, challenges, and future of additive manufacturing in engineering," *Comput.-Aided Des.*, vol. 69, pp. 65–89, Dec. 2015.
[2] E. Sachs, M. Cima, P. Williams, D. Brancazio, and J. Cornie, "Three dimensional printing: Rapid tooling and prototypes directly from a CAD model," *J. Eng. Ind.*, vol. 114, no. 4, pp. 481–488, Nov. 1992.
[3] J. Dumas, J. Hergel, and S. Lefebvre, "Bridging the gap: Automated steady scaffoldings for 3D printing," *ACM Trans. Graph.*, vol. 33, no. 4, p. 98, Jul. 2014.
[4] J. Vanek, J. A. G. Galicia, and B. Benes, "Clever support: Efficient support structure generation for digital fabrication," *Comput. Graph. Forum*, vol. 33, pp. 117–125, Aug. 2014.
[5] X. Zhang, X. Le, A. Panotopoulou, E. Whiting, and C. C. L. Wang, "Perceptual models of preference in 3D printing direction," *ACM Trans. Graph.*, vol. 34, no. 6, p. 215, Nov. 2015.
[6] K. Hu, S. Jin, and C. C. L. Wang, "Support slimming for single material based additive manufacturing," *Comput.-Aided Des.*, vol. 65, pp. 1–10, Aug. 2015.
[7] P. Herholz, W. Matusik, and M. Alexa, "Approximating free-form geometry with height fields for manufacturing," *Comput. Graph. Forum*, vol. 34, no. 2, pp. 239–251, 2015.
[8] A. Muntoni, M. Livesu, R. Scateni, A. Sheffer, and D. Panozzo, "Axis-aligned height-field block decomposition of 3D shapes," *ACM Trans. Graph.*, vol. 37, no. 5, p. 169, Nov. 2018.
[9] R. Hu, H. Li, H. Zhang, and D. Cohen-Or, "Approximate pyramidal shape decomposition," *ACM Trans. Graph.*, vol. 33, no. 6, p. 213, Nov. 2014.
[10] L. Luo, I. Baran, S. Rusinkiewicz, and W. Matusik, "Chopper: Partitioning models into 3D-printable parts," *ACM Trans. Graph.*, vol. 31, no. 6, p. 129, Nov. 2012.
[11] J. Vanek *et al.*, "PackMerger: A 3D print volume optimizer, " *Comput. Graph. Forum*, vol. 33, no. 6, pp. 322–332, 2014.
[12] W. Gao, Y. Zhang, D. C. Nazzetta, K. Ramani, and R. J. Cipra, "RevoMaker: Enabling multi-directional and functionally-embedded 3D printing using a rotational cuboidal platform," in *Proc. 28th Annu. ACM Symp. User Interface Softw. Technol.*, Nov. 2015, pp. 437–446.
[13] M. Yao, Z. Chen, L. Luo, R. Wang, and H. Wang, "Level-set-based partitioning and packing optimization of a printable model," *ACM Trans. Graph.*, vol. 34, no. 6, p. 214, Nov. 2015.
[14] X. Chen *et al.*, "Dapper: Decompose-and-pack for 3D printing," *ACM Trans. Graph.*, vol. 34, no. 6, p. 213, Nov. 2015.
[15] W. M. Wang, C. Zanni, and L. Kobbelt, "Improved surface quality in 3D printing by optimizing the printing direction," *Comput. Graph. Forum*, vol. 35, no. 2, pp. 59–70, May 2016.
[16] P. Song *et al.*, "CofiFab: Coarse-to-fine fabrication of large 3D objects," *ACM Trans. Graph.*, vol. 35, no. 4, p. 45, Jul. 2016.
[17] X. Wei *et al.*, "Toward support-free 3D printing: A skeletal approach for partitioning models," *IEEE Trans. Vis. Comput. Graphics*, vol. 24, no. 10, pp. 2799–2812, Oct. 2018.

[18] R. Schmidt and N. Umetani, "Branching support structures for 3D printing," in *Proc. ACM SIGGRAPH*, New York, NY, USA: ACM, Aug. 2014, p. 9.
[19] S. Keating and N. Oxman, "Compound fabrication: A multi-functional robotic platform for digital design and fabrication," *Robot. Comput.-Integr. Manuf.*, vol. 29, no. 6, pp. 439–448, Dec. 2013.
[20] Y. Pan, C. Zhou, Y. Chen, and J. Partanen, "Multitool and multi-axis computer numerically controlled accumulation for fabricating conformal features on curved surfaces," *J. Manuf. Sci. Eng.*, vol. 136, no. 3, 2014, Art. no. 031007.
[21] X. Song, Y. Pan, and Y. Chen, "Development of a low-cost parallel kinematic machine for multidirectional additive manufacturing," *J. Manuf. Sci. Eng.*, vol. 137, no. 2, 2015, Art. no. 021005.
[22] H. Peng, R. Wu, S. Marschner, and F. Guimbretière, "On-the-fly print: Incremental printing while modelling," in *Proc. CHI Conf. Hum. Factors Comput. Syst.*, May 2016, pp. 887–896.
[23] R. Wu, H. Peng, F. Guimbretière, and S. Marschner, "Printing arbitrary meshes with a 5DOF wireframe printer," *ACM Trans. Graph.*, vol. 35, no. 4, p. 101, Jul. 2016.
[24] J. Huang *et al.*, "Framefab: Robotic fabrication of frame shapes," *ACM Trans. Graph.*, vol. 35, no. 6, p. 224, Nov. 2016.
[25] C. Dai, C. C. L. Wang, C. Wu, S. Lefebvre, G. Fang, and Y.-J. Liu, "Support-free volume printing by multi-axis motion," *ACM Trans. Graph.*, vol. 37, no. 4, p. 134, Aug. 2018.
[26] A. V. Shembekar, Y. J. Yoon, A. Kanyuck, and S. K. Gupta, "Generating robot trajectories for conformal three-dimensional printing using nonplanar layers," *J. Comput. Inf. Sci. Eng.*, vol. 19, no. 3, 2019, Art. no. 031011.
[27] K. Xu, L. Chen, and K. Tang, "Support-free layered process planning toward 3 + 2-axis additive manufacturing," *IEEE Trans. Autom. Sci. Eng.*, vol. 16, no. 2, pp. 838–850, Apr. 2019.
[28] C. Wu, C. Dai, G. Fang, Y.-J. Liu, and C. C. Wang, "RoboFDM: A robotic system for support-free fabrication using FDM," in *Proc. IEEE Int. Conf. Robot. Autom. (ICRA)*, May 2017, pp. 1175–1180.
[29] B. T. Lowerre, "The harpy speech recognition system," Ph.D. dissertation, Dept. Comput. Sci., Carnegie Mellon Univ., Pittsburgh, PA, USA, 1976, Art. no. aAI7619331.
[30] P. Huang, C. C. L. Wang, and Y. Chen, "Algorithms for layered manufacturing in image space," in *Advances in Computers and Information in Engineering Research*. New York, NY, USA: ASME, 2014, pp. 377–410.
[31] Ultimaker. *Ultimaker Cura: Advanced 3D Printing Software, Made Accessible*. Accessed: Jun. 16, 2019. [Online]. Available: https://ultimaker.com/en/products/ultimaker-cura-software
[32] C. J. Kruit, "A novel additive manufacturing approach using a multiple degrees of freedom robotic arm," M.S. thesis, Fac. Mech., Maritime Mater. Eng. (3mE), Delft Univ. Technol., South Holland, The Netherlands, Aug. 2013.
[33] A. Makhal and A. K. Goins, "Reuleaux: Robot base placement by reachability analysis," in *Proc. 2nd IEEE Int. Conf. Robotic Comput. (IRC)*, Jan./Feb. 2018, pp. 137–142.

Chenming Wu received the B.Eng. degree in electronic information engineering from the Beijing University of Technology, Beijing, China, in 2015. He is currently pursuing the Ph.D. degree with the Department of Computer Science and Technology, Tsinghua University, Beijing.

His current research interests are intelligent design, computational fabrication, and robotics.

Chengkai Dai is currently pursuing the Ph.D. degree with the Department of Design Engineering, Delft University of Technology, Delft, The Netherlands.

His research area includes robotics, geometry computing, and computational design.

Guoxin Fang received the B.Eng. degree in mechanical engineering from the Beijing Institute of Technology, Beijing, China, in 2016. He is currently pursuing the Ph.D. degree with the Department of Design Engineering, Delft University of Technology, Delft, The Netherlands.

His research area includes advanced manufacturing, computational design, and robotics.

Yong-Jin Liu (M'13–SM'16) received the B.Eng. degree from Tianjin University, Tianjin, China, in 1998, and the Ph.D. degree from The Hong Kong University of Science and Technology, Hong Kong, in 2004.

He is currently a Professor with the Department of Computer Science and Technology, Tsinghua University, Beijing, China. His research interests include computational geometry, computer graphics, and computer-aided design.

Dr. Liu a member of ACM.

Charlie C. L. Wang (M'04–SM'11) received the Ph.D. degree in mechanical engineering from The Hong Kong University of Science and Technology, Hong Kong, in 2002.

He was a Tenured Professor and the Chair of Advanced Manufacturing with the Delft University of Technology (TU Delft), Delft, The Netherlands. He is currently a Professor of Mechanical and Automation Engineering and the Director of the Intelligent Design and Manufacturing Institute, The Chinese University of Hong Kong (CUHK), Hong Kong. His research areas include geometric computing, intelligent design, and advanced manufacturing.

Prof. Wang is currently a fellow of the American Society of Mechanical Engineers (ASME) and the Hong Kong Institute of Engineers (HKIE).